Eur Biophys J (2010) 39:971–977
DOI 10.1007/s00249-009-0465-6

ORIGINAL PAPER

Progressive pearl necklace collapse mechanism for cerato-ulmin aggregation film

F. Sbrana · D. Fanelli · M. Vassalli · L. Carresi · A. Scala · L. Pazzagli · G. Cappugi · Bruno Tiribilli

Received: 22 January 2009 / Revised: 21 April 2009 / Accepted: 29 April 2009 / Published online: 27 May 2009

Abstract Cerato-ulmin (CU) is a fungal toxin class II hydrophobin, involved in Dutch elm disease. The formation of hydrophobin films at the air–water interface is a key mechanism which plays a role of paramount importance at different stages of the fungal development. We present a study on the precursor stages of growth towards the self-assembly aggregation film of CU. Atomic force microscopy images of CU dropped on mica substrates indicate that the system self-organizes in almost one-dimensional pearl-necklace-like chains, which subsequently collapse and possibly merge to form extended and rather compact planar films. We propose and verify a simple model to describe the self-aggregation mechanism in terms of progressive thickening of the pearl chains due to the successive merging and collapse of the elementary constitutive units.

Keywords Protein aggregation · Cerato-ulmin · AFM · Persistence length · Chain

Proceedings of the XIX Congress of the Italian Society of Pure and Applied Biophysics (SIBPA), Rome, September 2008.

F. Sbrana · D. Fanelli · M. Vassalli · B. Tiribilli
CSDC, Dipartimento di Fisica, Università degli Studi di Firenze, Via Sansone 1, 50019 Sesto Fiorentino, Italy

D. Fanelli
Dipartimento di Energetica and INFN, Università degli Studi di Firenze, Via S. Marta 3, 50139 Florence, Italy

M. Vassalli · B. Tiribilli (✉)
Istituto dei Sistemi Complessi, Consiglio Nazionale delle Ricerche (CNR, ISC), Via Madonna del Piano 10, 50019 Sesto Fiorentino, Italy
e-mail: bruno.tiribilli@isc.cnr.it; bruno.tiribilli@gmail.com

M. Vassalli
Istituto di Biofisica, Consiglio Nazionale delle Ricerche, Via De Marini 6, 16149 Genoa, Italy

L. Carresi · A. Scala
Dipartimento di Biotecnologie Agrarie, Università degli Studi di Firenze, Via della Lastruccia, 10, 50019 Sesto Fiorentino, Italy

L. Pazzagli · G. Cappugi
Dipartimento di Scienze Biochimiche, Università di Firenze, Viale Morgagni 50, 50134 Florence, Italy

Introduction

In the history of plant pathology Dutch elm disease (DED) is one of the most devastating and destructive diseases. It is caused by the ascomycetes *Ophiostoma novo-ulmi* and *Ophiostoma ulmi*, and it is vectored by bark beetles. The disease firstly emerged in The Netherlands in 1919, and quickly spread to North Europe, reaching North America (Brasier 1988). In the 1990s *O. himal-ulmi*, a third species also very virulent to European elms, was found to occur in the western Himalayas in an apparent natural balance with the elms native there (Brasier and Mehrotra 1995). Many studies have contributed to elucidate the pathogenesis of DED, hypothesizing a correlation between DED fungi virulence and their capability to produce the protein cerato-ulmin (CU) by the fungi (Del Sorbo et al. 2002). A number of observations had led to assess the role of CU as the major virulence factor of DED pathogens, since it produced the same symptoms and morphological and physiological alterations as DED when injected into elm trees: wilting, lowering of transpiration, and increase in respiration of leaves (Takai 1974; Takai and Hiratsuka 1984; Del Sorbo et al. 2000). The toxin is secreted in the medium of shake cultures and was found to be a structural component of the hyphal surface of both *O. ulmi* and *O. novo-ulmi* (Tadesse

et al. 2003; Scala et al. 1997). The occurrence of CU in the cell wall renders the wall surface more hydrophobic, favoring the adhesion of the pathogen to the insect vector, and hence its dissemination and the spread of the disease; it also protects the fungus from dehydration (Temple and Horgen 2000). Recently, Carresi et al. (2008) have isolated the ortholog of the CU gene in *Ophiostoma quercus*, closely related to the DED fungi, and showed that the purified CU protein sequence was quite different from those of the other *Ophiostomas*. Surprisingly, a strain of *Geosmithia* sp., isolated from an *Ulmus minor* tree showing DED symptoms in southern Italy, possessed and expressed the CU gene, suggesting the possibility of CU gene horizontal transfer from the *Ophiostomas* in distant fungal species (Scala et al. 2007).

Cerato-ulmin is an 8-kDa protein (75 amino acids) phytotoxic hydrophobin which shows the typical hydropathic profile, solubility, and eight cysteine residues (arranged in a conserved pattern) of class II hydrophobins (Stringer and Timberlake 1993). Hydrophobins are small proteins, secreted as monomers by filamentous fungi, and share the presence of eight cysteine residues involved in four disulfide bridges. Moreover they self-assemble into amphipathic layer structures at hydrophilic–hydrophobic interfaces (Wösten and de Vocht 2000; Wösten 2001). On the basis of their hydropathy pattern hydrophobins can be classified into class I or II. Class I hydrophobin, such as SC3 from *Schizophyllum commune* (Wösten et al. 1993; Kwan et al. 2006) or Po.HYD1 from *Pleurotus ostreatus* (Ma et al. 2008), form rodlet-like surface pattern resistant to dissociation. The rodlets are structurally related to amyloid fibrils, are enriched in β-structure, and are able to interact with specific dyes (Sunde et al. 2008; Chiti and Dobson 2006). Further class II hydrophobin, such as HFBI and HFBII from *Trichoderma reesei* in dimer, trimer or tetramer aggregates, form highly organized planar compact film at water–air interface (Torkkeli et al. 2002; Hakanpää et al. 2004; Askolin et al. 2006). As all hydrophobins, CU proteins play an important role in the aerial hyphae formation. Once they reach an interface, they self-assemble, coating the hyphae fungal surface and so making the hyphae surface hydrophobic. Consequently they promote the escape of fungal hypha from hydrophilic environments and so its spread. In this scenario it is of interest to highlight the mechanism that regulates the spontaneous assembly aggregation film of CU at hydrophilic–hydrophobic interface.

In this work the CU aggregation is verified to be a hierarchical process in which semiflexible polymers, resembling pearl-necklace chains, as revealed by atomic force microscopy (AFM), progressively collapse, giving rise to larger beads, these latter being still arranged in chains. The process is spontaneously iterated until a uniform compact film is eventually formed.

Materials and methods

Chemicals and buffers

The semipreparative reverse-phase (RP) high-performance liquid chromatography (HPLC) column (C4, 5 µm, 250 × 10 mm) was from Phenomenex (Grace, Columbia, MD, USA).

The Sephadex LH-60 column was from Pharmacia (Uppsala, Sweden). The 0.45 µm membrane was from Millipore (Bedford, MA, USA). Malt Extract Agar was from Oxoid (Basingstoke, UK). Thioflavine T (ThT) and other chemical reagents were from Sigma (St. Louis, MO, USA).

Purification and aggregation of cerato-ulmin

Fungus culture

CU was isolated from liquid cultures of *O. novo-ulmi* 182 and H328. Fungi were routinely cultivated on malt extract agar (MEA) (Brasier 1981) or in liquid Takai medium (Takai and Richards 1978). For long-term storage, blastoconidia collected from 3-day-old liquid shaken minicultures (3 ml) in Takai medium were resuspended in 10% (vol/vol) glycerol and stored at −70°C.

Purification procedure

CU was purified from the cultural filtrate according to the procedure previously described by Scala et al. (1994) with some modifications. Briefly, fungal liquid culture was obtained by transferring an agar plug from a culture grown on MEA for 5–7 days at 23°C to 1 l Takai medium and it was kept at 25°C for 7 days. Culture filtrates were obtained by removing mycelia and spores from the medium after filtration through 0.45-µm Millipore membrane. The culture filtrate was then lyophilized and redissolved in 60% ethanol to have a 60-fold concentrated solution. The concentrated solution was clarified by centrifugation at 8,000*g* for 30 min. The supernatant was applied to a 3.6 × 120 cm Sephadex LH-60 column that was equilibrated and eluted with 60% ethanol at 3.2 ml/h. Five-milliliter fractions were collected and assayed for the presence of CU by a turbidimetric method of Takai and Richards (1978): 100 µl each chromatographed fraction was added to 1 ml water, the solution was vigorously vortexed, and the optical density was determined. The CU-containing fractions were pooled, vacuum dried, resuspended in 2 ml 60% ethanol, and rechromatographed on the same LH-60 column. The eluted fractions containing CU were collected, vacuum-dried, and dissolved in 5 ml 30% acetonitrile in water. CU was obtained in pure form after RP-HPLC chromatography on a

C-4 column (Phenomenex, 10 × 250 mm, 10 μm) which was eluted with a linear water/acetonitrile gradient. The purity and the molecular weight of the obtained CU were checked by sodium dodecyl sulfate polyacrylamide gel electrophoresis (SDS-PAGE) and matrix-assisted laser desorption/ionization time-of-flight (MALDI-TOF) mass spectrometry. The final yield was 3 mg pure protein starting from 1 l filtrate. Protein concentration was determined by amino acid analysis (Benson and Hare 1975).

Formation of CU assemblages

A 10 μM suspension of CU in water was kept under continuous stirring in a balancing shaker at 50 rpm/min at 25°C. Self-aggregation of CU was followed by fluorescence spectroscopy using ThT according to literature (Chiti and Dobson 2006; LeVine 1999). After 24 h, 50 μl of suspension was mixed with 450 μl 6.4 μM ThT in 50 mM glycine–NaOH buffer, pH 8.5. ThT fluorescence spectra were followed on a Perkin-Elmer LS-55 spectrofluorimeter using $\lambda_{ex} = 435$ nm and λ_{em} of 400–600 nm. Slits were set at 5 nm width in both the excitation and emission monochromators. Fluorescence of the soluble protein was also measured.

Atomic force microscopy

AFM analysis of the CU was performed in air at ambient conditions, in intermittent contact mode, using a PicoSPM microscope equipped with AAC-Mode controller and with a 100-μm scanner (Agilent, Santa Clara, CA). Scanner calibration was periodically checked by means of a reference grid (TGZ02 by MikroMash, Tallin, Estonia) with known pitch (3 μm) and step height (100 nm). Cantilever model NSG-01 (NT-MDT Co., Moscow, Russia) with 150 kHz typical resonance frequency and tip radius ≤10 nm were used. Images of 10 μm × 10 μm size were acquired using a scan rate of about 1 line/s. The sample was prepared by deposition of 2 μl suspension of aggregated CU onto a freshly cleaved mica disc. After 2 min, the sample was rinsed with a few drops of distilled water and dried overnight.

Image processing

AFM images were processed using WSxM (Horcas et al. 2007) software in order to remove the sample tilt in the data. The profile analysis function was used to measure the height and the width (s) of the chains. The fractal dimension (D) of the images was evaluated using the open-source software ImageJ (http://rsb.info.nih.gov/ij) on the basis of a standard box-counting algorithm applied to a binarized version of each image.

Moreover, 2D Single Molecules software (freeware—Nanostructured Materials Group Software. Clarkson University. Potsdam NY; Web: http://people.clarkson.edu/~sminko) was used in order to measure the contour length (L_c) and the persistence length (L_p) of collapsing chains according to literature (Frontali et al. 1979; Rivetti et al. 1996). The curve backbones of each chain were manually traced on the piece of the closing pearl chain by dragging a mouse cursor on the AFM image, and the spatial coordinates were recorded with 2 nm resolution.

Results and discussion

The modifications in the purification procedure enabled us to obtain a final yield of 3 mg pure CU starting from 1 l filtrate. In order to induce the formation of assemblages, a suspension of CU in water was allowed to self-aggregate under mild stirring at room temperature. Formation of aggregates was monitored by ThT, suggesting the appearance of partially ordered structures as evidenced by the maximum of the emission peak at 482 nm (Fig. 1). This is a particularly interesting observation as class II hydrophobins are in general not capable of interacting with standard dyes, commonly employed when aiming at monitoring the aggregation process of both amyloid and class I hydrophobins. This makes CU attractive candidates to investigate proteins' self-assembling properties. In fact, a remarkable functional property of CU proteins, and of all hydrophobins, has to do with their inherent ability to spontaneously self-aggregate in film, once they reach a hydrophilic–hydrophobic interface, hence coating the

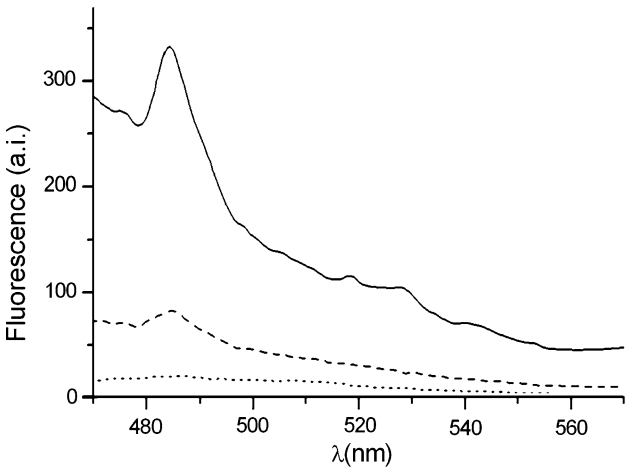

Fig. 1 Fluorescence spectra of ThT in the presence of CU aliquots: 10 μM CU in water was aggregated under stirring for 24 h; 50 μL (*solid line*) and 5 μL (*dashed line*) of the suspension were mixed with 450 and 495 μL, respectively, 6.4 μM ThT in 50 mM glycine buffer, pH 8.5. *Dotted line* ThT alone. The peak at 482 nm indicates the formation of ordered aggregates

hyphae surface and consequently modifying the associated hydrophobic characteristics. Moreover, CU is one of the few example of phytotoxic hydrophobin, and the characterization of its peculiar, ThT-positive aggregates can help in understanding the role of this protein in the host-microbe interaction.

To morphologically substantiate the aggregation of CU, we resorted to the AFM technique. We chose mica as substrate, a hydrophilic one, to mimic the hyphae surface. To induce aggregation, the protein in water solution was stirred, giving rise to a water–air interface, and so favoring the self-assembly mechanism. A continuous balancing movement, acting as an external perturbation, avoids the formation of a uniform film at the air/water interface on top of the suspension.

In Fig. 2a, a representative AFM image of CU deposition on mica is shown. Long, almost one-dimensional, chains are clearly observed. Visually, they look similar to pearl necklaces, being constituted of a sequence of adjacent beads. Zooming into the image allows us to appreciate some of the morphological details of such structures. Both the background uniform layer (Fig. 2b) and the pearl chains (Fig. 2d) appear to be constituted of protein agglomerate and so have analogous density. From the profile analysis, reported in Fig. 2c, the height of the chain with respect to the surrounding background results as 1.8 nm. This value is compatible with dimension of a CU monolayer as estimated by comparison with similar hydrophobins, such as HFBII (Hakanpää et al. 2004). It can hence be speculated that the chains are a single-layer assembly of CU proteins.

A gallery of 10 μm × 10 μm AFM images was collected by scanning randomly selected areas of the sample under scrutiny. In all cases, a rather uniform film was consistently observed as well as numerous dotted chains, bent in various shapes. These latter display however an apparently large variety of longitudinal and transverse sizes: experimental evidence which inspires the development of a unifying picture for the underlying aggregation process. As we shall substantiate in the following, a hierarchical aggregation is in fact believed to take place, which eventually yields the packed film, passing through the chains as intermediate steps. More specifically, a chain segment can occasionally bend, and so make its edges interact. The locally curled chain can further collapse, giving rise to a larger bead, which constitutes the fundamental unit for the successive level of aggregation. This process is ultimately expected to converge to the uniform substrate, as observed in the AFM experiments. A qualitative cartoon of the postulated mechanism is depicted in Fig. 3.

A morphology analysis of the AFM images was performed to shed light on the correctness of the proposed scenario. First, the fractal dimension was evaluated for each of the recorded AFM images. The fractal parameter was found to range from 1.35 to 1.57 for images characterized by a relatively sparse distribution of structures (Table 1). Conversely, the fractal dimension rapidly grows

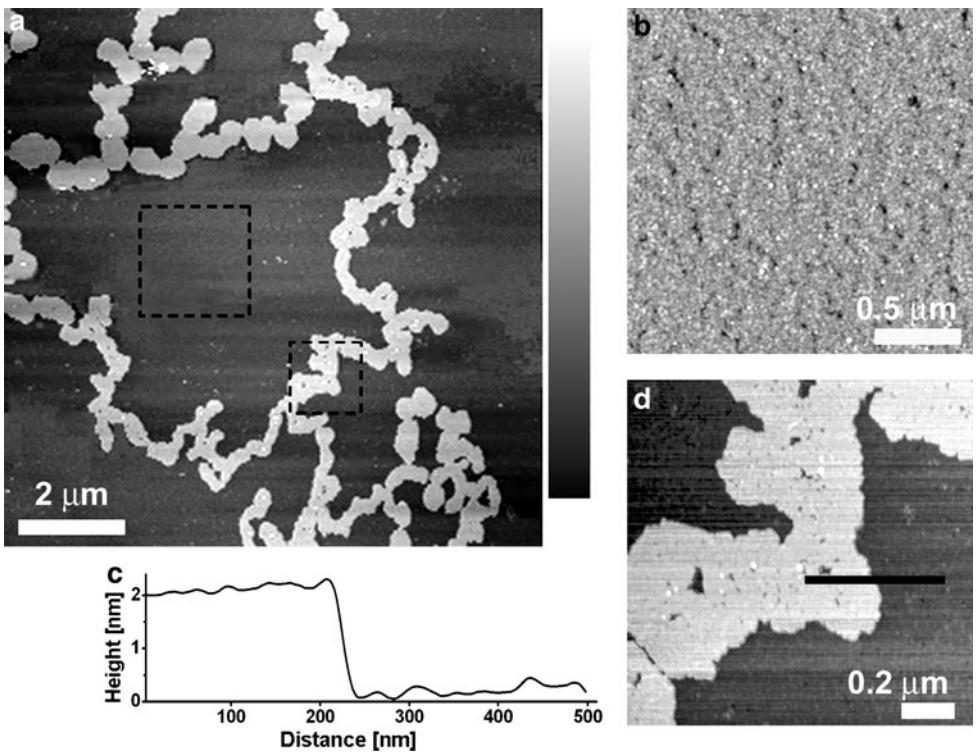

Fig. 2 **a** Representative AFM topography image of ceratoulmin deposition on freshly cleaved mica substrate. Both the background layer and the pearl necklace chains are clearly visible. Here, the image size is 10 μm × 10 μm, while the *z* range is 4.8 nm. **b** Zoom of *large dashed square* in image (**a**) to fully appreciate the background layer. A dense and uniform background layer of protein is visible. Image size is 2 μm × 2 μm. **c** Profile analysis from **d** (*black line*). The chain height is displayed with respect to the background layer (which hence is set the zero); the height difference is quantified as about 1.8 nm. **d** Zoom of *small dashed square* in image (**a**) on the pearl chain. Image size is 1.3 μm × 1.3 μm

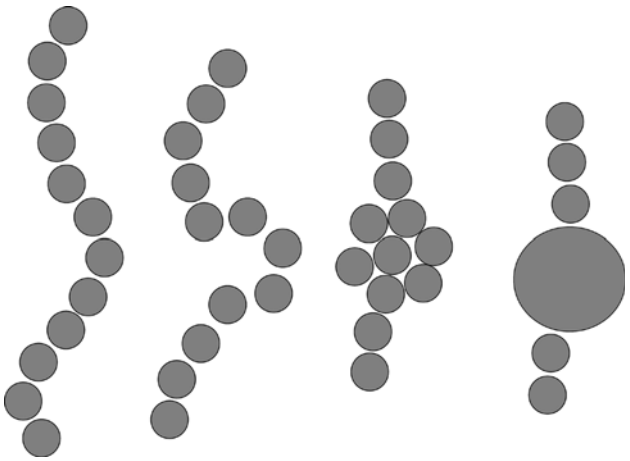

Fig. 3 From left to right, a scheme for the postulated progressive aggregation process: bending of the chain, two pearls come close, the curled segment collapses, and a new larger pearl is eventually formed

to 1.91 when the surface becomes almost uniformly covered (data not reported in Table 1). This is in agreement with the supposed progression from thin (almost one-dimensional, $D \approx 1$) chain, to fully coated surface ($D \approx 2$), via a complex sequence of intermediate structures.

To further characterize the aggregation mechanism, we quantitatively measured the width of the chains, hereafter denoted by s. An estimate of s was extracted by means of a dedicated profile analysis. Our attention was in particular aimed at the subset of chain segments rolling up into almost closed rings, as required within the interpretative framework postulated above. Moreover, and exploiting a semiflexible polymer description for the chain elements (Frontali et al. 1979), we also accessed a direct measure of the associated contour and persistence lengths. We here recall that L_p is defined as the length over which correlations in the tangent direction are lost; it returns an effective indication of the stiffness of the chain. In Table 1, the chain width and mean value of contour length (L_{cm}) are reported, as well as the corresponding persistence length, for all the AFM images analyzed. Interestingly, both s and L_{cm} are shown to increase with L_p.

In particular, as can be seen from Fig. 4, the chain width s is found to grow in discrete steps when plotted as a function of the L_p. A staircase pattern is observed in the progressive chain thickening. Three classes of necklace-like chains can be singled out, which for convenience are termed "small," "medium," and "large", respectively. In Fig. 5a–c, a representative AFM image for each of the selected classes is shown. The broadening of the chain can be clearly appreciated by visual inspection. In Fig. 5d, as a further step in the aggregation, large uniform islands are observed, being occasionally connected via tiny chains.

Table 1 Experimental data: persistence length (L_p), chain width (s), mean value of contour length (L_{cm}), and fractal dimension (D)

Image (no.)	L_p (nm)	s (nm)	L_{cm} (nm)	D
1	45	163	392	1.38
2	45	168	377	1.42
3	48	168	399	1.45
4	52	178	399	1.35
5	52	166	419	1.44
6	55	153	453	1.44
7	69	251	485	1.38
8	74	264	598	1.45
9	77	285	590	1.51
10	96	275	852	1.50
11	103	276	859	1.45
12	149	517	1,118	1.51
13	149	508	908	1.52
14	158	438	1,229	1.51
15	160	472	1,210	1.57
16	164	452	1,309	1.53
17	183	498	1,263	1.54

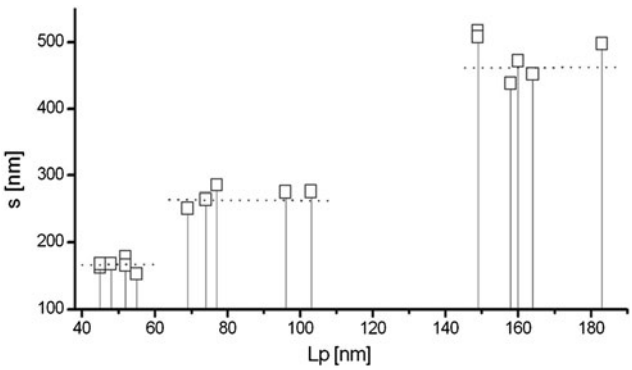

Fig. 4 Chain width s plotted as a function of persistence length (L_p) for each acquired AFM image. The staircase pattern signals progressive chain thickening. Interestingly, chain width increases in discrete steps. Three classes of necklace-like chains are consequently identified

Under our working ansatz, the aggregation mechanism of CU protein is a self-assembling process that goes through successive collapses. The pearls belonging to the class of large chains should therefore result from the evolution of the medium-class chain. A similar dynamical relation can be imagined to intimately link small and medium chains, respectively. Given the chain width (s) and the contour length (L_{cm}) at a given (small or medium) stage of evolution, it should hence be possible to infer its expected size at the next level (medium or large) of hierarchical clustering. The curled chain, which is about to become the next-level bead, occupies in fact an area A which totals:

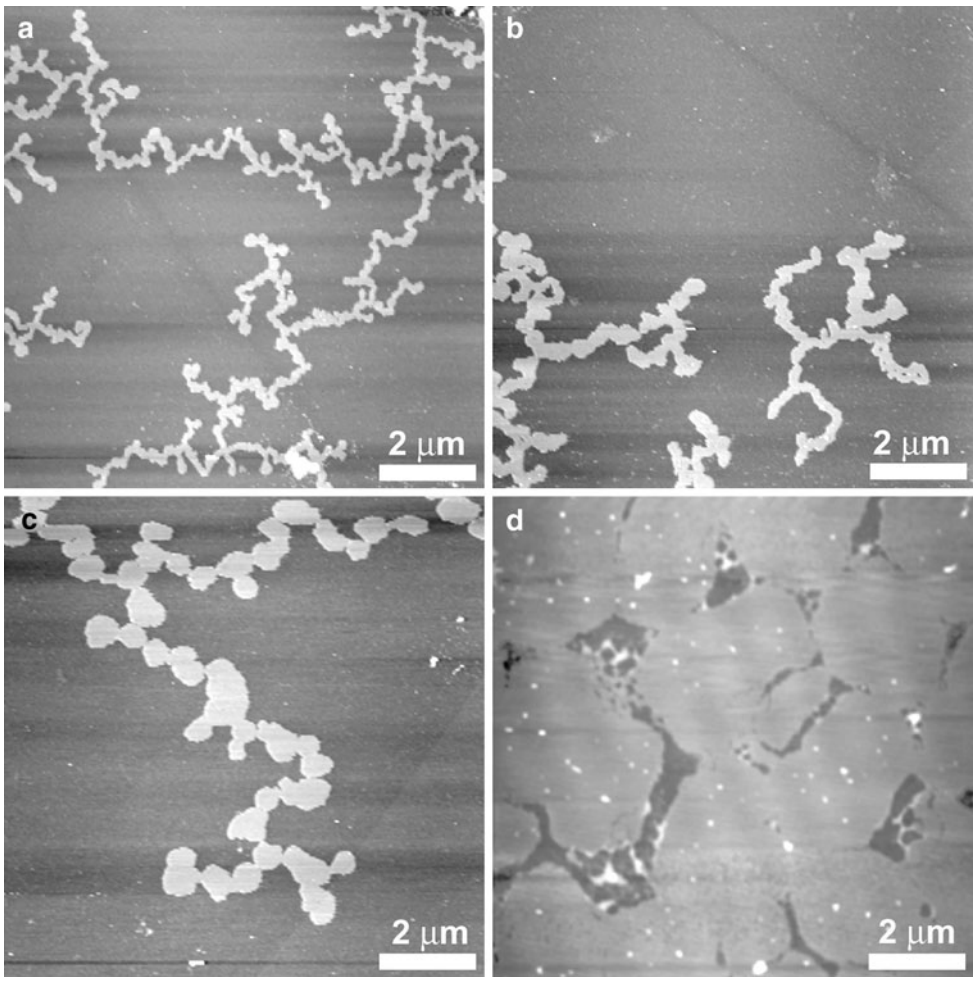

Fig. 5 Representative AFM topography images of ceratoulmin deposited on freshly cleaved mica substrate showing (**a**, **b**, **c**) progressive thickening of pearl necklace chains and (**d**) nearly complete coverage of substrate surface with large islands connected by occasionally chains. Image size (**a**, **b**, **c**, **d**) is 10 μm × 10 μm

Table 2 Comparison between the experimental and expected dimension values for small-, medium-, and large-class chains

Class	L_{cm} (nm)	s (nm)	d (nm)
Small	407	166	
Medium	677	270	293
Large	1,173	481	482

$$A = sL_{cm}, \tag{1}$$

the newborn bead being hence characterized by an average diameter, d, given by

$$d = 2\sqrt{\frac{L_{cm}s}{\pi}}. \tag{2}$$

The expected bead's diameter, calculated from the mean width and contour length according to the above relation, are reported in Table 2. Clearly, only medium and large units can be predicted on the basis of the preceding iterative reasoning. Excellent agreement is indeed found with a direct measure of the homologous quantities, an observation which confirms the adequacy of the proposed scenario.[1]

In summary, morphological analysis of AFM images of CU points to the ability of the system to spontaneously evolve from one-dimensional pearl-necklace-like chains towards extended planar film made of uniformly packed constituents. A simple geometrical argument is proposed herein, which governs the nested phases of the dynamical evolution. Our claims are in turn corroborated via a self-consistent benchmarking with direct AFM experiments. Additional studies are certainly needed to further elucidate the dynamical aspects of the suggested aggregation paradigm, as well as to clarify the role that mature aggregates may play in the actual physiological behavior of hyphae fungal surface and in the induction of DED pathogenesis.

[1] As a side remark, we notice that an alternative mechanism could be imagined where the chain segment closes into a ring, rather than a compact entity, the inner hole being subsequently filled with external addition of biological material. The calculation can be extended to account for this latter scenario, and returns an analogous degree of similarities between predicted and measured quantities (data not shown).

In particular it would be extremely important to access a time-resolved sequence of samples, aiming at eventually confirming the recursive aggregation mechanism here hypothesized on the basis of a purely deductive analysis. Future experiments are planned along these lines, which would provide an independent validation of the proposed scenario of structure formation.

References

Askolin S, Linder M, Scholtmeijer K, Tenkanen M, Penttilä M, de Vocht ML, Wösten HAB (2006) Interaction and comparison of a class I hydrophobin from *Schizophyllum commune* and class II hydrophobins from *Trichoderma reesei*. Biomacromolecules 7:1295–1301. doi:10.1021/bm050676s

Benson JR, Hare PE (1975) *O*-phthalaldehyde: fluorogenic detection of primary amines in the picomole range. Comparison with fluorescamine and ninhydrin. Proc Natl Acad Sci USA 72:619–622. doi:10.1073/pnas.72.2.619

Brasier CM (1981) Laboratory investigations on Ceratocystis ulmi. In: Stipes RJ, Campana RJ (eds) Compendium of elm diseases, vol 96. American Phytopathological Society, St. Paul, pp 76–79

Brasier CM (1988) Genetic systems in *Ophiostoma ulmi*. In: Sidhu GS (ed) Genetics of plant pathogens, vol 6. Advances in plant pathology, Academic, London, pp 207–223

Brasier CM, Mehrotra MD (1995) Ophiostoma himal-ulmi sp nov, a new species of Dutch elm disease fungus endemic to the Himalayas. Mycol Res 99:205–215. doi:10.1016/S0953-7562(09)80887-3

Carresi L, Comparini C, Bettini P, Pazzagli L, Cappugi G, Scala F, Scala A (2008) Isolation of the orthologue of the cerato-ulmin gene in *Ophiostoma quercus* and characterization of the purified protein. Mycol Res 112:1245–1255. doi:10.1016/j.mycres.2008.05.005

Chiti F, Dobson CM (2006) Protein misfolding, functional amyloid, and human disease. Annu Rev Biochem 75:333–366. doi:10.1146/annurev.biochem.75.101304.123901

Del Sorbo G, Scala F, Parrella G, Lorito M, Comparini C, Rocco M, Scala A (2000) Functional expression of the gene CU, encoding the phytotoxic hydrophobin cerato-ulmin, enables *Ophiostoma quercus*, a nonpathogen on elm, to cause symptoms of Dutch elm disease. Mol Plant Microbe Interact 13:43–53. doi:10.1094/MPMI.2000.13.1.43

Del Sorbo G, Scala A, Scala F, Tegli S (2002) Cerato-ulmin, a toxin produced by the pathogens of the Dutch elm disease. In: Upadhyay R (ed) Advances in microbial toxin research and its biotechnological exploitation, Kluwer Academic/Plenum, New York, pp 93–104

Frontali C, Dore E, Ferrauto A, Gratton E, Bettini A, Pozzan MR, Valdevit E (1979) An absolute method for the determination of the persistence length of native DNA from electron micrographs. Biopolymers 18:1353–1373. doi:10.1002/bip.1979.360180604

Hakanpää J, Paananen A, Askolin S, Nakari-Setälä T, Parkkinen T, Penttilä M, Linder MB, Rouvinen J (2004) Atomic resolution structure of the HFBII hydrophobin, a self-assembling amphiphile. J Biol Chem 279:534–539. doi:10.1074/jbc.M309650200

Horcas I, Fernandez R, Gomez-Rodriguez JM, Colchero J, Gomez-Herrero J, Baro AM (2007) WSXM: a software for scanning probe microscopy and a tool for nanotechnology. Rev Sci Instrum 78:013705. doi:10.1063/1.2432410

Kwan AH, Winefield RD, Sunde M, Matthews JM, Haverkamp RG, Templeton MD, Mackay JP (2006) Structural basis for rodlet assembly in fungal hydrophobins. Proc Natl Acad Sci USA 103:3621–3626. doi:10.1073/pnas.0505704103

LeVine H (1999) Quantification of the β-sheet amyloid fibril structures with Thioflavin T. Methods Enzymol 309:274–284. doi:10.1016/S0076-6879(99)09020-5

Ma AM, Shan LJ, Wang HJ, Du ZP, Xie BJ (2008) Partial characterization of a hydrophobin protein Po.HYD1 purified from the oyster mushroom *Pleurotus ostreatus*. World J Microbiol Biotechnol 24:501–507. doi:10.1007/s11274-007-9500-x

Rivetti C, Guthold M, Bustamante C (1996) Scanning force microscopy of DNA deposited onto mica: equilibration versus kinetic trapping studied by statistical polymer chain analysis. J Mol Biol 264:919–932. doi:10.1006/jmbi.1996.0687

Scala A, Tegli S, Comparini C, Mittempergher L, Scala F, Del Sorbo G (1994) Influence of fungal inoculum on cerato-ulmin production; purification of cerato-ulmin and detection in elm sucker cuttings. Petria 4:57–67

Scala F, Bertelli E, Coppola L, Del Sorbo G, Tegli S, Scala A (1997) Comparative determination of cerato-ulmin on cell surface and in mycelial extracts of pathogenic and non-pathogenic Ophiostoma species. Mycol Res 101:829–834. doi:10.1017/S0953756296003358

Scala A, Comparini C, Tegli S, Scala F (2007) A non-Ophiostoma fungus expresses the gene encoding the hydrophobin cerato-ulmin. J Plant Pathol 89:233–240

Stringer MA, Timberlake WE (1993) cerato-ulmin, a toxin involved in Dutch elm disease, is a fungal hydrophobin. Plant Cell 5:145–146

Sunde M, Kwan AH, Templeton MD, Beever RE, Mackay JP (2008) Structural analysis of hydrophobins. Micron 39:773–784. doi:10.1016/j.micron.2007.08.003

Tadesse Y, Bernier L, Hintz WE, Horgen PA (2003) Real time RT-PCR quantification and Northern analysis of cerato-ulmin (CU) gene transcription in different strains of the phytopathogens *Ophiostoma ulmi* and *O. novo-ulmi*. Mol Genet Genomics 269:789–796. doi:10.1007/s00438-003-0890-7

Takai S (1974) Pathogenicity and cerato-ulmin production in *Ceratocystis ulmi*. Nature 252:124–126. doi:10.1038/252124a0

Takai S, Hiratsuka Y (1984) Scanning electron microscope observations of internal symptoms of white elm following *Ceratocystis ulmi* infection and cerato-ulmin treatment. Can J Bot 62:1365–1371. doi:10.1139/b84-186

Takai S, Richards WC (1978) cerato-ulmin, a wilting toxin of *Ceratocystis ulmi*: isolation and some properties of cerato-ulmin from the culture of *C. ulmi*. J Phytopathol 91:129–146. doi:10.1111/j.1439-0434.1978.tb04205.x

Temple B, Horgen PA (2000) Biological roles for cerato-ulmin, a hydrophobin secreted by the elm pathogens, *Ophiostoma ulmi* and *O. novo-ulmi*. Mycologia 92:1–9. doi:10.2307/3761443

Torkkeli M, Serimaa R, Ikkala O, Linder M (2002) Aggregation and self-assembly of hydrophobins from *Trichoderma reesei*: low resolution structural models. Biophys J 83:2240–2247. doi:10.1016/S0006-3495(02)73984-2

Wösten HAB (2001) Hydrophobins: multipurpose proteins. Annu Rev Microbiol 55:625–646. doi:10.1146/annurev.micro.55.1.625

Wösten HAB, de Vocht ML (2000) Hydrophobins, the fungal coat unravelled. Biochim Biophys Acta 1469:79–86

Wösten HAB, de Vries OMH, Wessels JGH (1993) Interfacial self-assembly of a fungal hydrophobin into a rodlet layer. Plant Cell 5:1567–1574